J. Fluid Mech. (2017), *vol.* 825, *pp.* 1–15. © Cambridge University Press 2017
doi:10.1017/jfm.2017.280

A study of the asymmetric shock reflection configurations in steady flows

Yuan Tao[1], Weidong Liu[1,†], Xiaoqiang Fan[1], Bin Xiong[1], Jiangfei Yu[2] and Mingbo Sun[1]

[1]Science and Technology on Scramjet Laboratory, National University of Defense Technology, Changsha, 410073, PR China

[2]College of Aerospace Science and Engineering, National University of Defense Technology, Changsha, 410073, PR China

(Received 26 November 2016; revised 20 April 2017; accepted 23 April 2017; first published online 18 July 2017)

In this paper the asymmetric shock reflection configurations in two-dimensional steady flows have been studied theoretically. For an overall Mach reflection, it is found that the horizontal distance between both triple points in the Mach stem is related to the angles of two slip streams. Based on the features of the converging stream tube, several assumptions are put forward to perform better the wave configurations near the slip streams. Therefore, we present an analytical model here to describe the asymmetric overall Mach reflection configurations which agrees well with the computational and experimental results.

Key words: compressible flows, flow–structure interactions, shock waves

1. Introduction

It is generally known that shock reflection phenomena appear in many practical engineering applications, ranging from supersonic aircraft wings to hypersonic vehicles and engines. In steady flows, there exist two classical types of shock reflection configuration. One is called regular reflection (RR) and the other irregular reflection (IR). In general, IR refers commonly to a three-wave shock wave configuration (Mach reflection, MR).

Since Mach firstly observed two different shock reflection configurations in 1878, abundant research in this field has been carried out. Later, in the 1940s, the detachment criterion and the von Neumann criterion were proposed to describe the transition between MR and RR by von Neumann (1943, 1945), respectively. Based on the two transition criteria, the (M_0, θ_w)-plane (free-stream Mach number M_0 for the x axis and wedge angle θ_w for the y axis) could be divided into three domains: the regular reflection domain, Mach reflection domain and dual solution domain, shown in figure 1 (see Hornung, Oertel & Sandeman 1979; Chpoun *et al.* 1995; Ben-Dor 1999, 2007). Here, $\theta_w^D(M)$ is the detachment criterion and $\theta_w^N(M)$ the von Neumann criterion. Therefore, for a given combination of M_0 and θ_w, the possible types of shock reflection configuration could be predicted theoretically.

† Email address for correspondence: WDliu@nudt.edu.cn

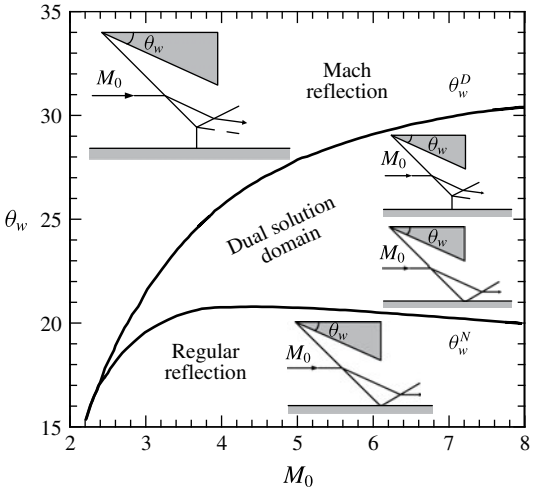

FIGURE 1. Domains of possible shock reflection configurations (data for the curves taken from Ben-Dor 2007, p. 77).

Further, regular reflection configurations could be well described with the inviscid two-shock theory and Prandtl–Meyer expansion theory. However, it is difficult to predict the Mach reflection configuration with these two theories due to the uncertainty in the Mach stem height. Azevedo & Liu (1993) assumed that the sonic throat formed by the converging stream tube behind the Mach stem, the slip stream and the leading expansion wave, which emanates from the trailing edge, meet at one point. Subsequently, Li & Ben-Dor (1997) developed a modified model, supposing that the flow direction of the slip stream at the sonic throat is parallel to the symmetric line. In this model, the reflected shock and the slip stream are slightly curved, due to the effect of expansion waves. Based on geometric considerations of the flow, Hornung & Mouton (2008), Mouton (2008), Mouton & Hornung (2008) presented a new approach for estimating the steady-state Mach stem height. Subsequently, taking the expansion waves and compression waves which exist over the slip stream into consideration, Gao & Wu (2010) proposed a new model which describes the Mach reflection configuration analytically and agrees very well with the computational fluid dynamics (CFD) numerical results. Also, Bai & Wu (2017) introduced the effect of secondary expansion waves and compression waves over the slip stream and presented the analytical expressions for the slip stream.

However, the above analytical models focus on the interactions of symmetric, rather than asymmetric shock waves that are more likely to occur in reality. Similar to the interaction of symmetric shock waves in steady flows, two types of shock reflection configuration may be formed when the interaction of asymmetric shock waves occurs. One is called overall regular reflection (oRR) and the other overall Mach reflection (oMR). Figure 2 clearly indicates that the oRR wave configuration consists of two RRs and the oMR wave configuration consists of two MRs. Chpoun & Lengrand (1997) conducted an initial experimental study on the reflection of asymmetric shock waves and thereby verified the existence of the asymmetric shock reflection hysteresis in the oRR $\leftrightarrow$ oMR transition. Li, Chpoun & Ben-Dor (1999) presented the theoretically possible wave configurations with the aid of shock polar combinations, and explained the physical nature of the asymmetric shock reflection hysteresis phenomenon. Then, a

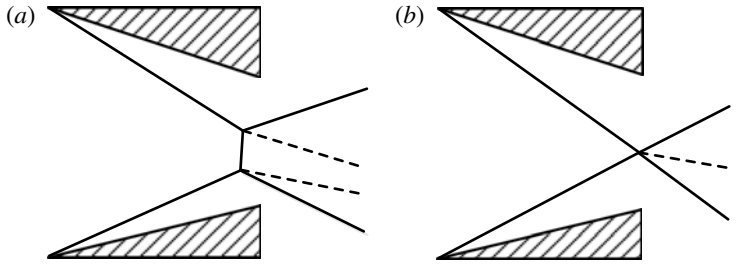

FIGURE 2. A schematic illustration of the possible overall wave configurations: (*a*) an overall Mach reflection (oMR), (*b*) an overall regular reflection (oRR).

series of experiments were carried out and verified their partial analytical results. Also, Ivanov *et al.* (2002) conducted a detailed numerical study, further verifying Li *et al.*'s theoretical findings. In addition, Hornung & Mouton (2008), Mouton (2008), Mouton & Hornung (2008) defined an equivalence shock angle to estimate the Mach stem height of the asymmetric shock reflection. In short, the above-mentioned theories made it possible to predict the type of overall wave configuration. Similarly to the regular reflections in steady flows, the entire flow field of overall regular reflections could be obtained by solving a series of governing equations. Note that owing to the flow complexity of the converging stream tube formed by two slip streams it is extremely difficult to describe the asymmetric overall Mach reflection configuration exactly.

Aiming to solve these problems, an analytical model is established, based on the previous contributions of many researchers. In § 2, we form several acceptable hypotheses on the shape of the asymmetric Mach stem according to Tao, Fan & Zhao's (2015) experimental results. Taking the features of the subsonic flow behind the Mach stem into consideration, we describe the asymmetric overall wave configurations analytically. Then, an analysis of the predicted results and previous results is described.

2. Physical model

The reflection of asymmetric shock waves in steady flows may be divided into two overall wave configurations: oRR and oMR. With a given combination of oncoming flow Mach number M_0 and two reflecting wedge angles θ_{w1}, θ_{w2}, the possible theoretical overall wave configurations could be obtained by using the shock polars. Since on both sides of the slip stream, the flows are parallel and the pressures are the same, the oRR wave configuration could be well established. Because of the existence of a subsonic region behind the asymmetric Mach stem, the difficulty of reappearance of the oMR wave configuration is increased.

2.1. *New features of oMR*

A schematic illustration of an asymmetric oMR wave configuration is displayed in figure 3(*a*). In the figure, the oMR configuration consists of two incident shocks (*IS* and *IS*′), two reflected shocks (*RS* and *RS*′), two slip streams (*SL* and *SL*′) and an asymmetric Mach stem (MS). H_w denotes the vertical distance between point *A* and point *C*. Also, *H* and H_g are the Mach stem height and the vertical distance between point *B* and point *D*, respectively. In addition, w_1 (w_2) is the wedge length and *L* denotes the relative position between two wedges.

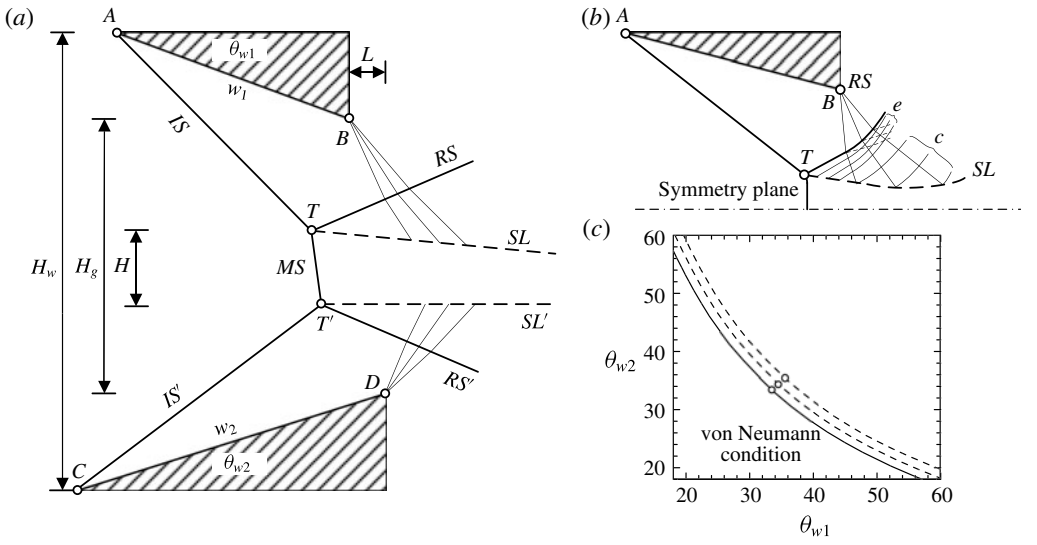

FIGURE 3. An overall Mach reflection (*a*) and Gao & Wu's symmetric Mach reflection configuration (*b*) and equivalence curves, with the ○ representing the symmetric cases (*c*).

Figure 3(*b*) shows an analytical Mach reflection configuration by Gao & Wu (2010). Comparatively speaking, there exist some new characteristics of the oMR configuration. First, the Mach stem MS may be asymmetric, which is induced by the difference in the wedge angles. Second, the flow direction in the stream tube behind the Mach stem is unknown. Third, it is quite difficult to simulate the interactions between the slip streams and several expansion waves, because they are asymmetric.

Hornung & Mouton (2008), Mouton (2008), Mouton & Hornung (2008) developed a theory to predict the asymmetric Mach stem height, shown in figure 3(*c*). In the figure, dashed lines denote equivalence curves, i.e. curves which are equidistant from the von Neumann condition (solid line). Then, the equivalence angle (the ○) can be determined, with a given combination of θ_{w1} and θ_{w2}. Although they defined an equivalence angle to estimate the Mach stem height in an overall Mach reflection, it should be noted that the effect of the relative position of the wedges on the Mach stem height is still ignored in this theory.

Considering the new features, an improved analytical model is proposed below.

2.2. *Wave interactions in oMR*

Gao & Wu (2010) pointed out that the flow region between the reflected shock and the slip stream is one filled with wave interactions. Similarly to the symmetric case, the wave interactions in this region can also be divided into two types, shown in figure 4. Both of these can be solved by using the previous theories. With Gao & Wu's (2010) analytical approach, we can hypothesize that the flow parameters ahead of the waves are known, i.e. data in region 1 and region 2. Then, the flow parameters behind the waves (data in regions 3, 4 and 5) can be obtained by solving a series of equations.

Figure 4(*a*) presents the interaction between the reflected shock wave *r* (*RS*/*RS*′) and the expansion wave *E* that emanates from the trailing edge of the reflecting wedge. Specifically, the reflected shock *r* interacts with an expansion wave *E* at point *R*,

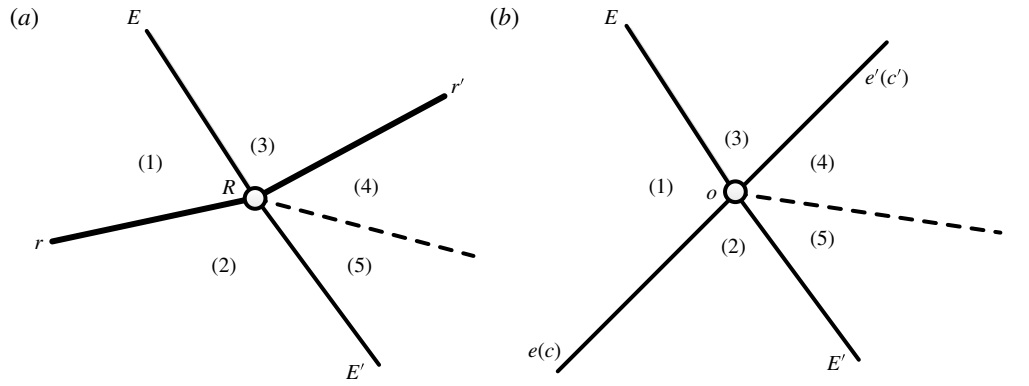

FIGURE 4. Schematic illustration of the wave interactions. (*a*) Type (a), a reflected shock r interacts with an expansion wave E, (*b*) type (b), an expansion wave e (compression wave c) interacts with an expansion wave E.

resulting in a refracted shock r', a refracted expansion wave E' and a slip stream (denoted by dashed line).

By using the Prandtl–Meyer relations, Mach number M, pressure P and flow direction θ in region 3 can be achieved. Note that subscripts 1, 2, 3, 4 and 5 refer to the flow states in the corresponding regions.

$$\theta_3 - \theta_1 = \nu(M_3) - \nu(M_1), \quad P_3/P_1 = \chi(M_1, M_3), \tag{2.1a,b}$$

where

$$\nu(M) = \sqrt{\frac{\gamma+1}{\gamma-1}}\arctan\left(\sqrt{\frac{(\gamma-1)(M^2-1)}{\gamma+1}}\right) - \arctan(\sqrt{M^2-1}), \tag{2.2}$$

$$\chi(M_0, M) = \left[\frac{2+(\gamma-1)M_0^2}{2+(\gamma-1)M^2}\right]^{\gamma/(\gamma-1)}. \tag{2.3}$$

Here, γ is the ratio of specific heats.

Similarly, we also can obtain the flow parameters in region 5,

$$\theta_5 - \theta_2 = \nu(M_5) - \nu(M_2), \quad P_5/P_2 = \chi(M_2, M_5). \tag{2.4a,b}$$

Considering that

$$P_4 = P_5, \quad \theta_4 = \theta_5, \tag{2.5a,b}$$

the Mach number M_4 and the shock angle of r' $\beta_{r'}$ can be obtained with the oblique shock relations. These equations are

$$M_4^2 = F(M_3, \beta_{r'}), \quad \theta_4 - \theta_3 = G(M_3, \beta_{r'}), \quad P_4/P_3 = J(M_3, \beta_{r'}), \tag{2.6a–c}$$

where

$$F(M, \beta) = \frac{M^2 + \dfrac{2}{\gamma-1}}{\dfrac{2\gamma}{\gamma-1}M^2\sin^2\beta - 1} + \frac{M^2\cos^2\beta}{\dfrac{\gamma-1}{2}M^2\sin^2\beta + 1}, \tag{2.7}$$

$$G(M,\beta)=\arctan\left(2\cot\beta\frac{M^2\sin^2\beta-1}{M^2(\gamma+\cos 2\beta)+2}\right), \tag{2.8}$$

$$J(M,\beta)=1+\frac{2\gamma}{\gamma+1}(M^2\sin^2\beta-1). \tag{2.9}$$

Thus, type (a) of figure 4(*a*) can be obtained.

Figure 4(*b*) displays another type of wave interaction. Specifically, the expansion wave e (compression wave c) induced by the evolution of the slip stream SL (SL') interacts with the expansion wave E emanating from the trailing edge of the wedge. Based on the above conclusions, the flow parameters in region 3 satisfy

$$\theta_3-\theta_1=\nu(M_3)-\nu(M_1),\quad P_3/P_1=\chi(M_1,M_3). \tag{2.10a,b}$$

In the same way, by using the Prandtl–Meyer function we get:

$$\left.\begin{array}{ll}\theta_2-\theta_1=\nu(M_2)-\nu(M_1), & P_2/P_1=\chi(M_1,M_2),\\ \theta_4-\theta_3=\nu(M_4)-\nu(M_3), & P_4/P_3=\chi(M_3,M_4),\\ \theta_5-\theta_2=\nu(M_5)-\nu(M_2), & P_5/P_2=\chi(M_2,M_5).\end{array}\right\} \tag{2.11}$$

Considering the features of slip stream, an additional relations are supplemented,

$$P_4=P_5,\quad \theta_4=\theta_5. \tag{2.12a,b}$$

By solving the equations (2.10)–(2.12), M, P and θ in region 3–5 can be obtained. Consequently, similar to the symmetric case, the flow parameters in the region between RS and SL (RS' and SL') can be solved and obtained.

2.3. *Mach stem shape*

For MR, Li & Ben-Dor (1997) pointed out that the Mach stem shape is slightly curved. Tan, Ren & Wu (2006) analytically proved, using the small disturbance theory, that the Mach stem is a circular arc. Then, the fine structure of Mach stem was well observed experimentally by Tao *et al.* (2015), using the nano-tracer planar laser scattering technique, shown in figure 5. In their experiments, the inflow Mach number M_∞ is 4, the inflow total pressure P_∞ 101 kPa and the wedge angles 25.7° (upper) and 20.9° (lower), respectively.

As measured from the photograph, the angle of SL θ_{up} is −8.4° and the angle of SL' θ_{down} is −1.0°. Further, we assume that the averaged flow deflection angle while fluid passing across the Mach stem, MS, is equal to the flow deflection angle formed across a strong shock (straight line TT'). In the figure, the angle of the straight line connected to two triple points (T, T') is −88.6°. By using the oblique shock wave relations, the calculated flow deflection angle θ_m across the MS could be obtained and the value is −4.9°. It is easy to notice that the calculated flow deflection angle is approximately equal to the averaged flow deflection angle, i.e. $\theta_m\approx(\theta_{up}+\theta_{down})/2$. Based on this, a simplified schematic of Mach stem configuration is abstracted and plotted, see figure 6.

As shown in figure 6, the interaction between two incident shocks IS, IS' would result in two reflected shocks RS, RS', two slip streams SL, SL' and a Mach stem, MS. Using the classical three-shock theory, it is easy to describe the flow fields near

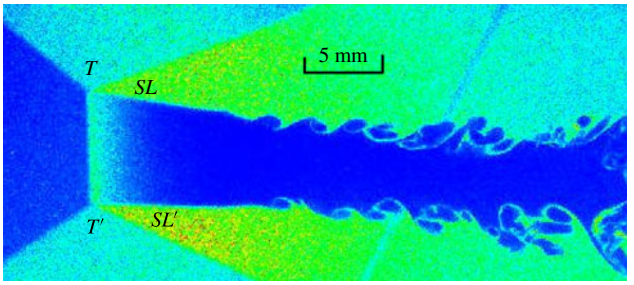

FIGURE 5. (Colour online) The fine structure of the oMR configuration (see Tao *et al.* 2015).

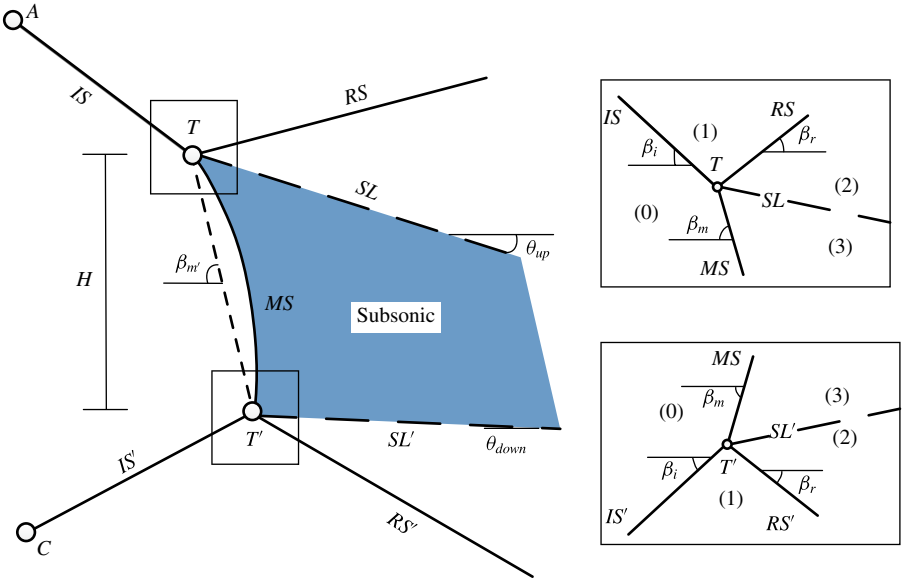

FIGURE 6. (Colour online) Schematic illustration of the Mach stem configuration.

both of the triple points T, T'. Hence, the flow parameters behind the shock waves could be expressed by the following equations:

$$\left.\begin{array}{ccc} M_1^2 = F(M_0, \beta_i), & \theta_1 = G(M_0, \beta_i), & P_1/P_0 = J(M_0, \beta_i), \\ M_2^2 = F(M_1, \beta_r), & \theta_2 = \theta_1 + G(M_1, \beta_r), & P_2/P_1 = J(M_1, \beta_r), \\ M_3^2 = F(M_0, \beta_m), & \theta_3 = G(M_0, \beta_m), & P_3/P_0 = J(M_0, \beta_m), \\ & P_2 = P_3, \quad \theta_2 = \theta_3. & \end{array}\right\} \tag{2.13}$$

Here, β_i, β_r and β_m denote the incident shock angle, the reflected shock angle and the angle of Mach stem, respectively. Subscripts 0, 1, 2 and 3 still refer to the flow states in the corresponding region separately. Then, the angles of the slip streams θ_{up}, θ_{down} could be obtained. Based on the foregoing discussion, the initial flow deflection angle θ_m across MS can be expressed as:

$$\theta_m = (\theta_{up} + \theta_{down})/2. \tag{2.14}$$

Consequently, the angle $\beta_{m'}$ of line TT' can be obtained using the oblique shock relation,

$$\theta_m = G(M_0, \beta_{m'}). \tag{2.15}$$

In addition, point A and point C are the leading edge points of the reflecting wedges and their coordinates in the (x, y)-coordinates system are (x_A, y_A) and (x_C, y_C), respectively. For a given vertical distance H between two triple points, the coordinates of T and T' can be expressed as:

$$\left.\begin{gathered} x_T = \frac{\tan\beta_{m'}H - \tan\beta_{m'}y_A - \tan\beta_2 H + \tan\beta_{m'}\tan\beta_1 x_A + \tan\beta_{m'}y_c - \tan\beta_{m'}\tan\beta_2 x_c}{\tan\beta_{m'}(\tan\beta_1 - \tan\beta_2)}, \\ y_T = \tan\beta_1(x_T - x_A) + y_A, \\ x_{T'} = x_T - H/\tan\beta_{m'}, \\ y_{T'} = y_T - H. \end{gathered}\right\} \tag{2.16}$$

2.4. *The flow in the subsonic pocket*

For the oMR configurations, it is difficult to describe the flow in the subsonic pocket analytically because of the uncertainty of the flow direction. In order to describe the flow state behind the Mach stem MS, several assumptions are made in our model.

In many instances, it is a valid approximation to neglect viscous effects along the slip stream completely. Therefore, we assume that the flow in the subsonic pocket is isentropic and quasi-one-dimensional, ignoring the flow deflection. It should be noticed that the actual flow parameters at any cross-section along the flow direction are not the same. Considering that the zone of dependence at any position in subsonic flows is the whole subsonic region, we assume that the averaged flow direction at any cross-section is merely related to the flow directions on the two sides of the slip stream.

The subsonic region before the leading characteristic line interacts with the slip streams is sketched, see figure 7. In the figure, symbols T, T' denote two triple points and lines TU_n, $T'V_n$ denote slip streams. Based on (2.14), the cross-sections which are perpendicular to the flow direction (TT_1 and $T'T_1'$) can be obtained. And, U_1 and V_1 are midpoints of TT_1' and T_1T', respectively. Therefore, U_1V_1 is defined as the entrance cross-section, and its sectional height is H_1,

$$H_1 = \frac{H_{m1} + H_{m2}}{2}. \tag{2.17}$$

Here, H_{m1} and H_{m2} are the length of TT_1 and $T'T_1'$, respectively.

The height of the throat H_s can be expressed as

$$\frac{H_1}{H_s} = \sigma(\overline{M}), \quad \sigma(M) = \frac{1}{M}\left(1 + \frac{\gamma - 1}{2}M^2\right)^{(\gamma+1)/(2\gamma-2)}. \tag{2.18}$$

Here, $\overline{M}$ is the averaged Mach number behind MS, i.e.

$$\overline{M}^2 = F(M_\infty, \beta_m'). \tag{2.19}$$

Besides, the averaged pressure $\overline{P}$ along the U_1V_1 line is

$$\overline{P} = J(M_\infty, \beta_m') \cdot P_\infty. \tag{2.20}$$

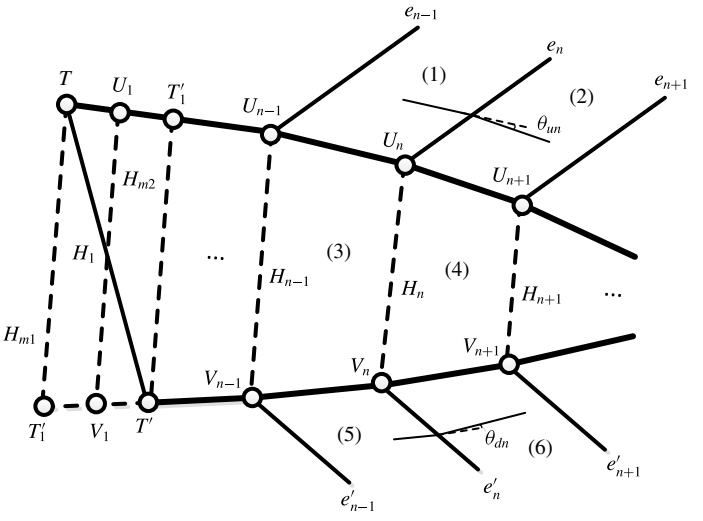

FIGURE 7. Schematic illustration of the subsonic region that is not affected by expansion fan.

Gao & Wu (2010) indicated that the pressure decreases along the stream tube, resulting in expansion waves. Subscripts 1–6 still refer to the flow states in corresponding regions. The flow parameters behind e_n and e_n' can be calculated using the following equations,

$$\theta_{un} = \theta_2 - \theta_1 = \nu(M_2) - \nu(M_1), \quad P_2/P_1 = \chi(M_1, M_2), \tag{2.21a,b}$$

$$\theta_{dn} = \theta_6 - \theta_5 = \nu(M_6) - \nu(M_5), \quad P_6/P_5 = \chi(M_5, M_6), \tag{2.22a,b}$$

$$P_3 = P_1 = P_5 = (P_{H_{n-1}} + P_{H_n})/2, \quad P_4 = P_2 = P_6 = (P_{H_n} + P_{H_{n+1}})/2, \tag{2.23a,b}$$

where

$$P_{H_i} = \chi(\overline{M}, \overline{M_i}) \cdot \overline{P}(i = 1, 2, \ldots n, \ldots). \tag{2.24}$$

Here, the averaged Mach number $\overline{M_i}$ at U_iV_i can be obtained using the quasi-one-dimensional steady relation,

$$\frac{H_i}{H_s} = \sigma(\overline{M_i})(i = 1, 2, \ldots n, \ldots), \tag{2.25}$$

where H_i is the length of U_iV_i $(i = 1, 2, 3 \ldots)$ and P_{H_i} denotes the pressure at the cross-section U_iV_i.

Based on the above, the averaged flow directions in region 3 $(U_{n-1}V_{n-1}V_nU_n)$ and region 4 $(U_nV_nV_{n+1}U_{n+1})$ are expressed as follows,

$$\theta_3 = (\theta_1 + \theta_5)/2, \quad \theta_4 = (\theta_2 + \theta_6)/2. \tag{2.26a,b}$$

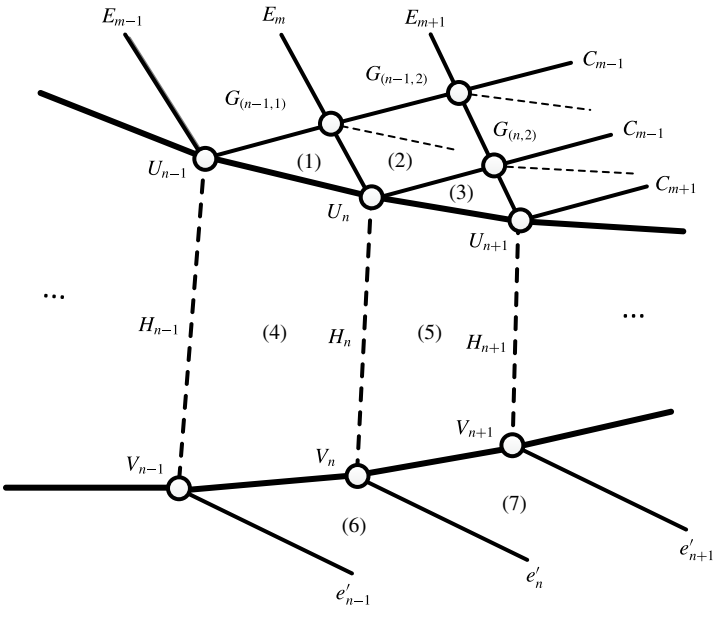

FIGURE 8. Schematic illustration of the subsonic region where one side is affected by the expansion fan.

In the (x, y)-coordinate system, the coordinates of U_i, V_i are (x_{u_i}, y_{u_i}), (x_{v_i}, y_{v_i}), $i = 1, 2, \ldots$. Then, several geometric relations are supplemented as follow,

$$\left.\begin{aligned} x_{u_n} &= x_{u_{n-1}} + \Delta x, \quad y_{u_n} = y_{u_{n-1}} + \Delta x \cdot \tan\theta_1, \\ x_{u_{n+1}} &= x_{u_n} + \Delta x, \quad y_{u_{n+1}} = y_{u_n} + \Delta x \cdot \tan\theta_2, \end{aligned}\right\} \tag{2.27}$$

$$\left.\begin{aligned} &\frac{y_{v_n} - y_{v_{n-1}}}{x_{v_n} - x_{v_{n-1}}} = \tan\theta_5, \quad \frac{y_{v_n} - y_{v_{n+1}}}{x_{v_n} - x_{v_{n+1}}} = \tan\theta_6, \\ &\frac{y_{v_n} - y_{u_n}}{x_{v_n} - x_{u_n}} = \tan(\pi/2 + \theta_3), \quad \frac{y_{v_{n+1}-y_{u_{n+1}}}}{x_{v_{n+1}} - x_{u_{n+1}}} = \tan(\pi/2 + \theta_4). \end{aligned}\right\} \tag{2.28}$$

Here, Δx is an arbitrary finite value.

Combining (2.17) with (2.28), the flow parameters of the region before the leading characteristic line of the expansion fan can be solved.

Figure 8 shows the wave configuration of the subsonic region and the evolution of one slip stream is affected by the expansion fan. On the one side of the stream tube, expansion waves interact with a slip stream, resulting in compression waves c. On the other side, several expansion waves, which are induced by the evolution of the other slip stream, occur. In the same way, the flow states of regions (3, 5, 7) and the positions of point U_{n+1} and point V_{n+1} can be obtained.

Specifically, the flow parameters in regions 3 and 7 are expressed, using the Prandtl–Meyer relations, as

$$\theta_3 - \theta_2 = \nu(M_3) - \nu(M_2), \quad P_3/P_2 = \chi(M_2, M_3), \tag{2.29a,b}$$

$$\theta_7 - \theta_6 = \nu(M_7) - \nu(M_6), \quad P_7/P_6 = \chi(M_6, M_7). \tag{2.30a,b}$$

Based on the features of slip streams, we can obtain,

$$P_1 = P_3 = P_6 = (P_{H_{n-1}} + P_{H_n})/2, \quad P_3 = P_5 = P_7 = (P_{H_n} + P_{H_{n+1}})/2, \quad (2.31a,b)$$

$$\theta_4 = (\theta_1 + \theta_6)/2, \quad \theta_5 = (\theta_3 + \theta_7)/2. \quad (2.32a,b)$$

In the same way, the coordinate of $G(n, 2)$ is $(x_{g_{(n,2)}}, y_{g_{(n,2)}})$. When the interaction between the expansion fan and the slip stream occurs in the upper side, the angle of $G_{(n,2)}U_{n+1}$ (β_{n1}) is $(\theta_3 - \arcsin 1/M_3)$. And when it occurs in the lower side, the value is $(\theta_3 + \arcsin 1/M_3)$. Therefore, the relations between the point U_{n+1} and the points U_n, $G_{(n,2)}$ can be established as,

$$\frac{y_{u_{n+1}} - y_{g_{(n,2)}}}{x_{u_{n+1}} - x_{g_{(n,2)}}} = \tan \beta_{n1}, \quad \frac{y_{u_{n+1}} - y_{u_n}}{x_{u_{n+1}} - x_{u_n}} = \tan \theta_3. \quad (2.33a,b)$$

Similarly, the following geometric relations are added,

$$\frac{y_{u_{n+1}} - y_{v_{n+1}}}{x_{u_{n+1}} - x_{v_{n+1}}} = \tan (\theta_5 + \pi/2), \quad \frac{y_{v_{n+1}} - y_{v_n}}{x_{v_{n+1}} - x_{v_n}} = \tan \theta_7. \quad (2.34a,b)$$

By solving (2.29)–(2.34), we can perfectly describe the interaction process displayed in figure 8.

In addition, the expansion fans emanating from the trailing edges may have a direct physical impact on the slip streams on both sides of the subsonic pocket, and this interaction is sketched in figure 9. The flow parameters in region 3 and region 6 can still be expressed as follows,

$$\theta_3 - \theta_2 = \nu(M_3) - \nu(M_2), \quad P_3/P_2 = \chi(M_2, M_3), \quad (2.35a,b)$$

$$\theta_6 - \theta_5 = \nu(M_6) - \nu(M_5), \quad P_6/P_5 = \chi(M_5, M_6). \quad (2.36a,b)$$

Note that there is a short distance between the cross-sections V_jV_j' and U_iU_i', the complexity of this problem for solving the downstream flow states is increased greatly. In order to simplify the analytical model, we assume that points V_j' and U_i' are located on the extended lines of $U_{i-2}U_{i-1}$ and $V_{j-1}V_j$, respectively.

When V_jV_j' is the upstream cross-section relative to U_iU_i', it is necessary to calculate the flow states in region $V_jV_{j+1}F_{(j,2)}$ first.

Then, the pressures on both sides of the slip stream V_jV_{j+1} satisfy the following condition,

$$P_6 = (P_{H_n} + P_{H_{n+1}})/2. \quad (2.37)$$

The averaged flow deflection angle $\theta_{v_{j+1}}$ at the cross-section $V_{j+1}V_{j+1}'$ is

$$\theta_{v_{j+1}} = (\theta_1 + \theta_6)/2. \quad (2.38)$$

The angle of line $F_{(j,2)}V_{j+1}$ (β_{j1}) is

$$\beta_{j1} = \theta_6 + \arcsin \frac{1}{M_6}. \quad (2.39)$$

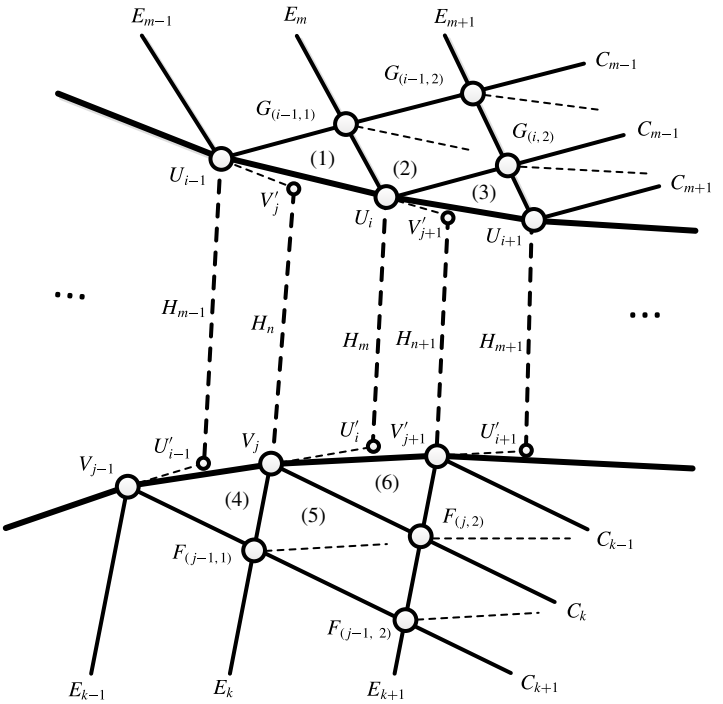

FIGURE 9. Schematic illustration of the subsonic region where both sides are affected by the expansion fans.

Considering that the coordinate of $F(j, 2)$ is $(x_{f_{(j,2)}}, y_{f_{(j,2)}})$, several geometric relations are added as follows,

$$\frac{y_{v_{j+1}} - y_{f_{(j,2)}}}{x_{v_{j+1}} - x_{f_{(j,2)}}} = \tan \beta_{j1}, \quad \frac{y_{v_{j+1}} - y_{v_j}}{x_{v_{j+1}} - x_{v_j}} = \tan \theta_6, \tag{2.40a,b}$$

$$\frac{y_{v'_{j+1}} - y_{v_{j+1}}}{x_{v'_{j+1}} - x_{v_{j+1}}} = \tan (\theta_{v_{j+1}} + \pi/2). \tag{2.41}$$

Using (2.36)–(2.41), the position of point V_{j+1} can be obtained. Then, the location of the new cross-section $V_{j+1}V'_{j+1}$ is compared with that of $U_iU'_i$. If $V_{j+1}V'_{j+1}$ is still the upstream cross-section relative to $U_iU'_i$, the forgoing procedure (2.30)–(2.41) is repeated for several cycles until VV' becomes the downstream cross-section relative to $U_iU'_i$. In addition, we have to obtain the flow parameters in region $U_iU_{i+1}G_{(i,2)}$. In the same way, a series of equations can be listed below,

$$P_3 = (P_{H_m} + P_{H_{m+1}})/2, \tag{2.42}$$

$$\theta_{u_{i+1}} = (\theta_3 + \theta_6)/2, \tag{2.43}$$

$$\beta_{i1} = \theta_3 - \arcsin \frac{1}{M_3}, \tag{2.44}$$

$$\frac{y_{u_{j+1}} - y_{g_{(i,2)}}}{x_{u_{i+1}} - x_{g_{(i,2)}}} = \tan \beta_{i1}, \quad \frac{y_{u_{i+1}} - y_{u_i}}{x_{u_{i+1}} - x_{u_i}} = \tan \theta_3, \tag{2.45a,b}$$

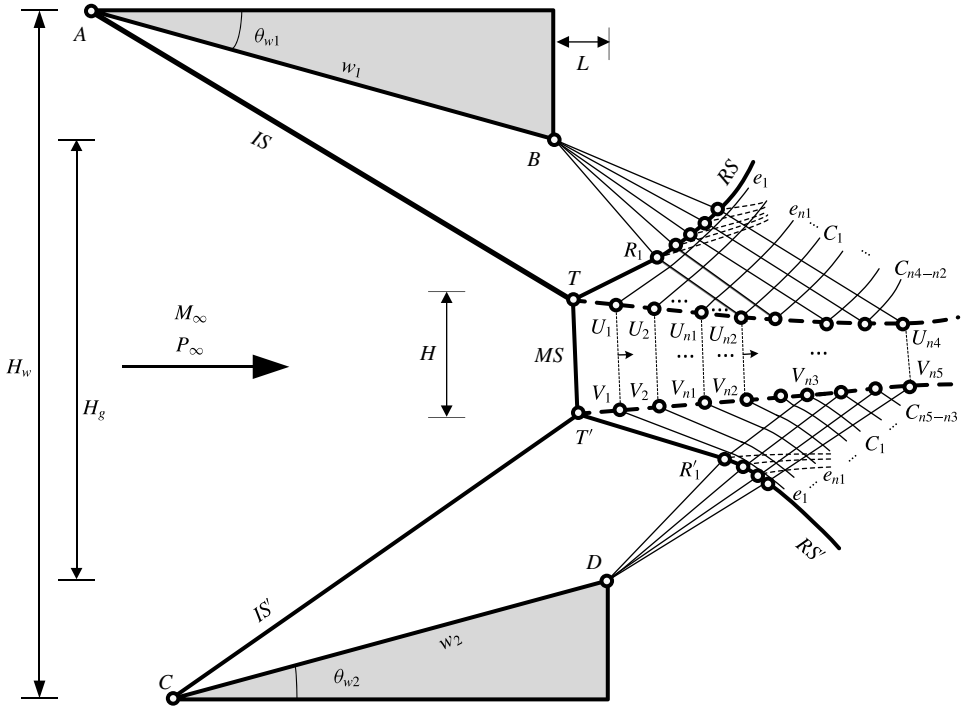

FIGURE 10. Schematic illustration of an overall Mach reflection.

$$\frac{y_{u'_{i+1}} - y_{u_{i+1}}}{x_{u'_{i+1}} - x_{u_{i+1}}} = \tan\left(\theta_{u_{i+1}} + \pi/2\right). \tag{2.46}$$

Here, β_{i1} is the angle of line $G_{(i,2)}U_{i+1}$ and $\theta_{u_{i+1}}$ is the angle of the averaged flow direction at $U_{i+1}U'_{i+1}$.

Finally, the schematic illustration of an oMR can be well presented and is shown in figure 10. In addition, the relation regarding the sonic throat is performed, i.e. the flow directions of slip streams on the two sides of the tube at the sonic throat are the same. Therefore, the minimum height of the cross-section along the flow direction H_s^* can be achieved. If $H_s^* \neq H_s$, we need to update the initial guess value of H.

2.5. *Discussion*

Table 1 gives the comparison of the Mach stem configuration between the present analytical results and the previous CFD results. For symmetric conditions (row a and row b), the analytical Mach stem height H_{the}/H_w agrees very well with Gao & Wu's (2010) CFD result H_{num}/H_w. Note that both of H_{the} and H_{num} are the vertical distances between two triple points and β_{the} and β_{num} indicate the angle of the straight line connected by two triple points. Therefore, it is easy to understand that β_{the} and β_{num} are both 90°. Furthermore, we can expect that the Mach stem height increases when $w_1/H_g(w_2/H_g)$ is increased. So H_{the}/H_w in row b is larger than that in row a.

For the asymmetric conditions, Kudryavstsev, Khotyanosky & Ivanov (2000) presented the hysteresis phenomenon that exists in the transition between oRR and oMR. During the hysteresis process, a series of asymmetrical shock reflection

No.	$w_1/H_g(w_2/H_g)$	θ_{w1}	θ_{w2}	H_{num}/H_w	H_{the}/H_w	β_{num}	β_{the}
a	1.14	28	28	0.283	0.289	90°	90°
b	1.19	28	28	—	0.3058	—	90°
c	1.19	28	24	0.1892	0.1982	$-89° \pm 0.5°$	−89.5°
d	1.19	28	18	0.0485	0.0596	$-88° \pm 0.5°$	−87.8°
e	1.19	36	18	0.2917	0.2980	$-86° \pm 0.5°$	−85.9°

TABLE 1. Mach stem height for various conditions at $M_0 = 4.96$, $L/H_w = 0$.

No.	$w_1/H_g(w_2/H_g)$	L/H_g	θ_{w1}	θ_{w2}	H_{exp}/H_w	H_{the}/H_w
a	2.53	0.0591	21.93	20.99	0.027	0.0274
b	2.56	0.0665	23.67	20.90	0.055	0.548
c	2.61	0.0758	25.89	20.73	0.099	0.981
d	2.60	0.0764	26.12	21.08	0.106	0.103
e	2.63	0.0871	28.43	20.90	0.146	0.127

TABLE 2. Mach stem height for various conditions at $M_0 = 4$.

configurations are displayed numerically. From rows c, d and e in table 1, it is observed that there is a relatively good agreement between the numerical and the theoretical results of the overall Mach reflection configuration. Specifically, it is shown that excellent agreement between β_{the} and β_{num} can be observed. Furthermore, the non-dimensionalized Mach stem height H_{the}/H_w predicted by this model agrees with results of Kudryavstsev *et al.* (2000), though the theoretical value is slightly larger than the numerical value.

The Mach stem height results for various wedges are presented in table 2. From the table, current theoretical results H_{the} agree with the previous experimental results H_{exp} of Hornung & Mouton (2008), Mouton (2008), Mouton & Hornung (2008). The experimental work of Mouton & Hornung shows slightly higher Mach stem heights than the corresponding ones in the current theoretical work.

3. Conclusions

In conclusion, we have studied the asymmetric shock reflection configurations in steady supersonic flows. On one hand, the overall regular reflection wave configurations can be well established by the current model, because the flow directions are consistent and the pressures are the same on both sides of the slip stream.

On the other hand, it is somewhat powerless to predict the overall Mach reflection wave configurations using the previous analytical models for Mach reflection. Accordingly, the symmetrical reflection model has been extended to an asymmetrical one. Specifically, we abstracted the shape of the Mach stem wave MS from Tao *et al.*'s (2015) experimental results and assumed an average slip angle to fix the direction of the quasi-one-dimensional duct. This model is capable of predicting the Mach stem height with good comparison to the previous numerical and experimental data.

Acknowledgements

This work was supported by National Natural Science Foundation of China NSFC grant 11372347, 11572347, 51406233, which was gratefully acknowledged.

REFERENCES

AZEVEDO, D. J. & LIU, C. S. 1993 Engineering approach to the prediction of shock patterns in bounded high-speed flows. *AIAA J.* **31**, 83–90.

BAI, C. Y. & WU, Z. N. 2017 Size and shape of shock waves and slipsline foe Mach reflection in steady flow. *J. Fluid Mech.* **818**, 116–140.

BEN-DOR, G. 1999 Hysteresis phenomena in shock wave reflections in steady flows. *J. Mater. Process. Technol.* **85**, 15–19.

BEN-DOR, G. 2007 *Shock Wave Reflection Phenomena*. Springer.

CHPOUN, A. & LENGRAND, J. C. 1997 Confirmation experimentale d'un phenomene d'hysteresis lors de l'interaction de deux chocs obliques de familles differentes. *C. R. Acad. Sci. Paris* **324** (1), 1–8.

CHPOUN, A., PASSEREL, D., LI, H. & BEN-DOR, G. 1995 Reconsideration of oblique shock wave reflections in steady flows. Part 1. Experimental investigation. *J. Fluid Mech.* **301**, 19–35.

GAO, B. & WU, Z. N. 2010 A study of the flow structure for Mach reflection in steady supersonic flow. *J. Fluid Mech.* **656**, 29–50.

HORNUNG, H. G. & MOUTON, C. A. 2008 Some more on transition between regular and Mach reflection of shock waves. In *38th Fluid Dynamics Conference and Exhibit, Washington, USA*, AIAA.

HORNUNG, H. G., OERTEL, H. & SANDEMAN, R. J. 1979 Transition to Mach reflection of shockwaves in steady and psuedo-steady flow with and without relaxation. *J. Fluid Mech.* **90**, 541–547.

IVANOV, M. S., BEN-DOR, G., ELPERIN, T., KUDRYAVTSEV, A. N. & KHOTYANOVSKY, D. V. 2002 The reflection of asymmetric shock waves in steady flows: a numerical investigation. *J. Fluid Mech.* **496**, 71–87.

KUDRYAVSTSEV, A. N., KHOTYANOSKY, D. V. & IVANOV, M. S. 2000 Numerical simulation of asymmetrical steady shock wave interactions. In *European Congress on Computational Methods in Applied Science and Engineering, Barcelona, Spain*.

LI, H. & BEN-DOR, G. 1997 A parametric study of Mach reflection in steady flows. *J. Fluid Mech.* **341**, 101–125.

LI, H., CHPOUN, A. & BEN-DOR, G. 1999 Analytical and experimental investigations of the reflection of asymmetric shock waves in steady flows. *J. Fluid Mech.* **390**, 25–43.

MOUTON, C. A. 2008 Transition between regular reflection and Mach reflection in the dual-solution domain. PhD thesis, California Institute of Technology.

MOUTON, C. A. & HORNUNG, H. G. 2008 Experiments on the mechanism of inducing transition between regular and Mach reflection. *Phys. Fluids* **20**, 126103.

VON NEUMANN, J. 1943 Oblique reflection of shocks. *Explosive Research Rep.* 12. Navy Department, Bureau of Ordnance, Washington, DC.

VON NEUMANN, J. 1945 Refraction, intersection and reflection of shock waves. *NAVORD Rep.* 203-245. Navy Department, Bureau of Ordnance, Washington, DC.

TAN, L. H., REN, Y. X. & WU, Z. N. 2006 Analytical and numerical study of the near flow field and shape of the Mach stem in steady flows. *J. Fluid Mech.* **546**, 341–364.

TAO, Y., FAN, X. Q. & ZHAO, Y. L. 2015 Flow visualization for the evolution of the slip stream in steady shock reflection. *J. Vis.* **18**, 21–24.